The Vagabond Fluorine Atom: Dissociative Photoionization of *trans*-1,3,3,3-Tetrafluoropropene

Amelia W. Ray[a], Peter Weidner[a], Andras Bodi,[b] Bálint Sztáray[a,*]

[a]*Department of Chemistry, University of the Pacific, Stockton, CA 95211, USA*

[b]*Laboratory for Synchrotron Radiation and Femtochemistry, Paul Scherrer Institute, CH-5232 Villigen PSI, Switzerland*

[*]Corresponding author: bsztaray@pacific.edu

Abstract

The dissociative photoionization of *trans*-1,3,3,3-tetrafluoropropene (HFO-1234ze) was investigated by imaging photoelectron photoion coincidence (PEPICO) spectroscopy. From the threshold photoelectron spectrum (TPES), an adiabatic ionization energy of 10.91 ± 0.05 eV is determined and reported for the first time. Over a 4-eV wide range, internal-energy selected *trans*-1,3,3,3-tetrafluoropropene cations decay by three parallel dissociative photoionization channels, which were modeled using statistical theory. The 0 K appearance energies of CF_2CHCF_2 (H-loss, *m/z* 113), $CFHCHCF_2$ (F-loss, *m/z* 95), and $CH_2{=}CF_2$ (CF_2-loss, *m/z* 64) fragment ions were determined to be 12.247 ± 0.030, 12.66 ± 0.10, and 12.80 ± 0.05 eV, respectively. From the last, the heat of formation of neutral *trans*-1,3,3,3-tetrafluoropropene was determined to be –779.9 ± 9.7 kJ/mol. While the lowest-energy fluorine loss occurs directly, the first H-loss and CF_2-loss channels involve both a fluorine- and a hydrogen-migration prior to dissociation. At higher internal energies, several other rearrangement pathways open up, which involve fluorine and hydrogen transfer and, through fluorine loss, lead to the formation of several additional isomeric allylic fragment ions.

Introduction

The propellant *trans*-1,3,3,3-tetrafluoropropene (HFO-1234ze) is a fourth-generation man-made refrigerant used today in spray dusters and other commercial applications. Earlier generations of man-made refrigerants, although effective for their intended purpose as refrigerants, propellants, and degreasers, were rife with unintended environmental consequences. Most notably, first-generation chlorofluorocarbons (CFCs) as well as their second-generation replacement, long-lived hydrochlorofluorocarbons (HCFCs), are well-known anthropogenic sources of reactive chlorine in the stratosphere.[1] These ozone-depleting species were ultimately phased out by the Montreal Protocol, after which stratospheric ozone concentrations have rebounded.[2] Currently, most commercial applications use third-generation hydrofluorocarbons (HFCs), more environmentally friendly alternatives due to their low ozone-depleting potential (ODP). However, even this generation is now subject to restrictions in the 2016 Paris Accord due to high global-warming potential (GWP) as a result of high absorption in the atmospheric window and long atmospheric lifetimes.[3,4] Accordingly, fourth-generation unsaturated HFCs, or hydrofluoroolefins (HFOs), with high gas-phase reactivity and consequent short atmospheric lifetimes and thus low GWPs, are an active field of development and research.

One such HFO of interest is *trans*-1,3,3,3-tetrafluoropropene, which was developed and introduced to the commercial market only recently as a refrigerant and propellant and has not yet been well studied. Previous studies focused largely on its liquid-phase thermochemical properties[3] and its estimated GWP and ODP.[5-7] Photolysis and kinetics studies of its reaction with OH, O_2, and O_3 suggested an estimated atmospheric lifetime of only 10–20 days;[4,8-11] such a favorably short lifetime implies that its estimated ODP is close to zero. Additionally, although *trans*-1,3,3,3-tetrafluoropropene does readily absorb IR radiation in the atmospheric window (700–1400 cm^{-1}),[4] its short atmospheric lifetime means its GWP is considered negligible as well. Negligible GWP and ODP values make this species an ideal replacement for more stable, saturated earlier-generation propellants.

The photoionization spectrum and dissociative photoionization of *trans*-1,3,3,3-tetrafluoropropene have not yet been documented in literature, so it may be constructive to look at the dissociation dynamics of the nearest analogs: propene (C_3H_6) and hexafluoropropene (C_3F_6). The (photo)ionization and dissociative (photo)ionization of the nearest perhydro-analog, propene, has been studied by both electron impact mass spectrometry (EI)[12,13] and photoionization mass spectrometry (PI).[14-16] Direct dissociation pathways include the loss of hydrogen or the breaking of the sigma C–C bond to produce either $C_2H_3^+$ or CH_3^+. Several rearrangement pathways have also been observed, including the loss of H_2, H_2 + H, and C_2H_2. The nearest perfluoro- analog, hexafluoropropene (C_3F_6), has been studied by photoionization mass spectrometry[17,18] and threshold photoelectron photoion coincidence (PEPICO) spectroscopy.[19] Unlike the related saturated perfluoropropane (C_3F_8) and similar to the unsaturated tetrafluroethylene,[20] C_3F_6 has a bound parent ion in the Franck–Condon region but exhibits large geometry change upon ionization, resulting in a threshold photoelectron spectrum with broad,

unresolved features and an ionization energy of 10.60 ± 0.03 eV.[17,19] Observed dissociation fragments include the four parallel channels $C_3F_5^+$ (F-loss), $C_2F_4^+$ (CF_2-loss), CF_3^+ (C_2F_3-loss), and CF^+ (C_2F_5-loss), and a consecutive channel leading to $CF^+ + C_2F_4 + F$ at higher dissociation energies.[19] Whether dissociation proceeds by formation of cyclic-C_3F_6[18] or by F-migration coupled with a lengthening of the sigma bond prior to dissociation,[19] the CF_2-loss channel must involve some form of rearrangement. Interestingly, F_2 loss in hexafluoropropene, equivalent to the prominent H_2 loss in propene, is absent. This is consistent with earlier PEPICO studies on fluorinated ethene cations[20] that show that substituting fluorine can dramatically change the dissociation dynamics due to the stronger C–F bonds, the presence of heavier fluorine, and inductive effects as a result of fluorine's increased electronegativity.

As a partially fluorinated propene system, *trans*-1,3,3,3-tetrafluoropropene also serves as a nice extension to an earlier PEPICO study of mono-, di-, tri-, and per-fluoroethene.[20] For these smaller fluorinated systems, five main dissociation channels were observed: HF-loss, statistical and non-statistical F-loss, cleavage of the C–C bond post H- or F-atom migration, and cleavage of the C=C bond. In monofluoroethene and 1,1-difluoroethene, the parent ions have long lifetimes before impulsive loss of HF with a large kinetic energy release due to significant reverse barriers to HF loss. In contrast, in C_2F_4, the two main channels at low energies involve C–C cleavage following F/H-transfer in which the charge stays on either fragment, leading to a self-consistent set of thermochemical values for the $CF/CF_3/CF^+/CF_3^+$ system.

In this paper, we describe threshold PEPICO spectroscopy measurements of *trans*-1,3,3,3-tetrafluoropropene over the photon range 10.8–15.0 eV. The threshold photoelectron spectrum and an adiabatic ionization energy of 10.91 ± 0.05 eV are reported for the first time. Dissociative photoionization in the studied energy range results in three ions: *m/z* 113 (H-loss), *m/z* 95 (F-loss), and *m/z* 64 (CF_2-loss). These dissociation pathways are plotted as fractional abundances and are modeled using RRKM theory to determine the lowest-energy dissociation pathway for each channel and to extract precise appearance energies for each fragment ion. The experimental work is complemented by *ab initio* calculations at the G4 level of theory on all stationary points of interest. Finally, we report, for the first time, experimental 0 K heats of formation values for the neutral precursor, its molecular ion and an allylic cation fragment.

Methods

PEPICO Experiments

Experiments were carried out on the CRF-PEPICO endstation of the VUV beamline at the Swiss Light Source, Paul Scherrer Institute.[21] As the spectrometer has been described in detail elsewhere,[22] only a short overview is provided here. A liquid sample of *trans*-1,3,3,3-tetrafluoropropene (HFO-1234ze) was placed in a glass vial from a spray duster (Elix Clean brand) at room temperature and the vapor was sampled from the headspace and introduced into the ionization region of the CRF-PEPICO with a typical chamber pressure of 1.3×10^{-6} mbar. Isolated

molecules were ionized by monochromatic VUV synchrotron radiation within a cross-section of 2 mm × 2 mm. Prior to interaction with the sample, the VUV synchrotron radiation was collimated, dispersed in grazing incidence by a laminar grating (600 grooves/mm), and focused at the exit slit in a differentially pumped gas filter containing a 10 mbar mixture of Ne and Ar to remove higher-order harmonics. The VUV radiation was calibrated using Ar autoionization lines at the first and second order of the grating. Experimental data was taken by scanning the photon energy from 10.8 to 15.0 eV, with a step size of 3 meV.

After ionization, photoelectrons and photoions were extracted in opposite directions using a constant 220 V cm^{-1} electric field and detected in coincidence. Photoelectrons were velocity-map-imaged (VMI) onto a Roentdek DLD40 position-sensitive delay-line detector, with an electron kinetic energy resolution of better than 1 meV at threshold. Photoions were mass analyzed using a gridless two-stage Wiley-McLaren time-of-flight (TOF) setup made up of 2.7 cm extraction, 8.7 cm acceleration, and 88.6 cm field-free drift regions. Photoions were also detected by a fast Roentdek DLD40 delay-line imaging detector. Data was collected using a multiple-start-multiple-stop coincidence data acquisition scheme where photoelectrons serve as a start signal and photoions as stop signal.[23] Threshold electrons were detected in the center of the VMI detector (where electron energy resolution is highest) and the contribution of "hot" electrons in the center (those ejected with non-zero velocity but no off-axis velocity component) was accounted for by subtracting the average count rate in a ring area surrounding the center, scaled by a factor that accounts for the area ratio of the two regions.[24] The fractional abundances of ions in coincidence with threshold photoelectrons were plotted as a function of photon energy to produce the breakdown diagram.

The combination of low extraction voltage and long extraction region results in ion residence times on the order of microseconds. While fast dissociation of the molecular ion will produce symmetric daughter peaks, slow dissociation in the extraction region will produce a fragment ion appearing somewhere between the TOF of the parent ion and the fragment ion. Daughter ions produced from a metastable parent will therefore appear in the time-of-flight spectra with a broad, quasi-exponential peak shape toward higher *m/*z.[25,26] Dissociation rates in the range 10^3–10^7 s^{-1} can be measured by fitting the modeled curves to the experimental TOF peak shapes, quantifying the kinetic shift.[27] However, in the case of a hydrogen loss from the parent ion, such as from $C_3H_2F_4^+$, the small difference in mass and, therefore, small time-of-flight difference between parent and daughter fragment ions is on the order of the instrumental peak width. Although the pseudo-exponential shape in the daughter ion TOF will be obscured in such cases, rate information can still be extracted using the shifting center of mass of the TOF peaks as a function of photon energy.[28,29] Therefore, in this work, the TOF peaks were fit using Gaussian functions to yield the fractional ion abundances for the breakdown curve and rate information was obtained from the experimental center of mass of the TOF peaks.[30]

Theoretical Methods

Analysis of the experimental data was aided by *ab initio* calculations carried out using the Gaussian 09 suite of programs.[31] Minimum structures for the neutral precursor, parent ion, and possible fragments were first optimized at B3LYP/6-311++G(d,p) level of theory. Transition state (TS) structures for the dissociative pathways were located by constrained optimizations (for loose TS with no saddle point), by scanning along the reaction coordinate, and by Synchronous Transit-Guided Quasi-Newton (STQN) calculations.[32,33] These TS structures were then verified to lead to the appropriate reactants and products (or intermediates) by intrinsic reaction coordinate (IRC) calculations.[34] Finally, more accurate energetics for the stationary points on the potential energy surface were determined by the G4 composite method.[35] For dissociation pathways where no reverse barrier was found, transition state structures were approximated by freezing the dissociating bond at 3.5 Å and performing a constrained optimization. Rotational constants and harmonic vibrational frequencies from these calculations were used in the statistical model to calculate the thermal energy distribution of the neutral precursor as well as the numbers and densities of states for the rate calculations.

Statistical Modeling

The experimental breakdown diagram and threshold TOF mass spectra were modeled within the Rice–Ramsperger–Kassel–Marcus (RRKM) framework for ionic dissociation reactions.[25,36] The thermal energy distribution of the neutral precursor molecule, its density, and the number of states and internal energy distribution of intermediate fragments were calculated using vibrational frequencies and rotational constants determined by *ab initio* calculations, *vide supra*. The RRKM unimolecular rate constants for each dissociation pathway, *k(E)*, were calculated as follows:

$$k(E) = \frac{\sigma N^{\ddagger}(E - E_0)}{h\rho(E)}$$

where σ is the symmetry number of the fragmentation channel, h is Planck's constant, $N^{\ddagger}(E - E_0)$ is the number of states of the transition state at internal energy $E - E_0$, and $\rho(E)$ is the density of states of the dissociating ion at internal energy E. The sums and densities of states were calculated using harmonic vibrational frequencies and the Beyer–Swinehart direct-count algorithm.[37] The transitional frequencies and the 0 K appearance energies of the model were then optimized to fit the experimental breakdown diagram and, in the case of the first metastable channel, the center-of-mass data.

Results and Discussion

1. Threshold Photoelectron Spectrum

The threshold photoelectron spectrum (TPES) of *trans*-1,3,3,3-tetrafluoropropene over the photon energy range 10.5–15.0 eV is shown in Figure 1. The spectrum consists of resolved peaks from 10.8 to 11.8 eV. The TPES spectrum was fit by Franck–Condon (FC) simulation, convoluted with Gaussians with a full width at half maximum of 100 cm^{-1}. An experimental adiabatic ionization energy (AIE) of 10.91 ± 0.05 eV was determined by offsetting the FC fit to fit the first three prominent peaks and adjusting the G4-calculated value of 10.899 eV accordingly.

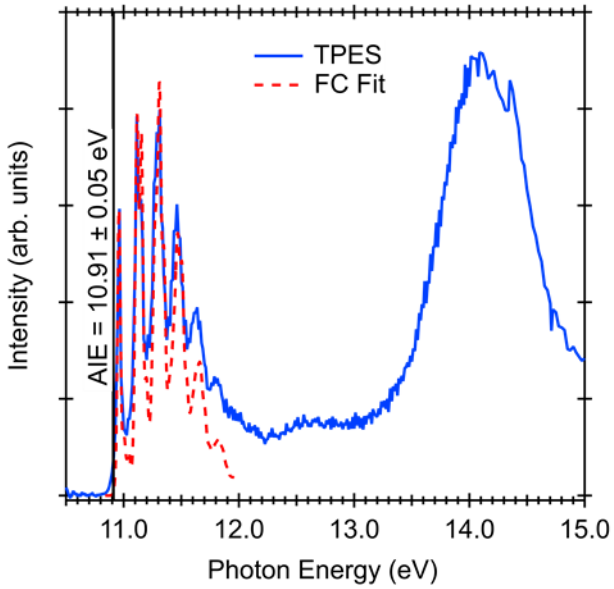

Figure 1. Threshold photoelectron spectrum of trans-1,3,3,3-tetrafluoropropene (blue) in the range 10.5–15.0 eV. Experimental data was fit using a Franck–Condon simulation (red).

2. Dissociative Photoionization Processes and Statistical Modeling

Threshold photoionization TOF mass spectra of energy-selected *trans*-1,3,3,3-tetrafluoropropene cations were measured over the photon energy range 11.8–15.0 eV. The fractional abundances of the molecular and fragment ion peak areas are plotted as a function of photon energy in the breakdown diagram shown in Figure 2. Only three fragment ions are observed in this energy range: *m/z* 113, *m/z* 95, and *m/z* 64. The *m/z* 113 fragment is readily attributed to the loss of a hydrogen atom; the *m/z* 95 fragment corresponds to the loss of a fluorine atom. The *m/z* 64 fragment cannot be formed by a direct bond scission in the parent ion; rather, based on mass, this fragment corresponds to the loss of a neutral CF_2 fragment. Previous work on hexafluoropropene[19] also observed this fragmentation pathway, and the stability of neutral CF_2 is well-established.[17,38]

A statistical thermodynamics model fit to the experimental data was used to obtain reaction rates and energy distributions for the lowest energy channels in the dissociative photoionization of *trans*-1,3,3,3-tetrafluoropropene, shown in Figure 2. The model used our

experimental AIE value of 10.91 ± 0.05 eV and a sample temperature of 300 K. In general, the 0 K appearance energy, E_0, corresponds to the dissociative photoionization energy (the thermochemical limit) in the absence of a reverse barrier; otherwise, E_0 corresponds to the energy of the rate-limiting transition state. The best fit was obtained by optimizing appearance energies (E_0's) and varying transition state transitional frequencies. Each fragmentation process was modeled using only the lowest-energy channel, and the experimental data is well fit by the model until 13.5 eV. Experimental appearance energies and fragment identifications for the lowest-energy dissociative pathways are summarized in Table 1; dissociation mechanisms are further explored by *ab initio* quantum chemical calculations in Section 3. The deviation in the model at higher energies strongly indicates the presence of additional dissociative pathways. While such higher-energy fragmentation pathways are clearly present, their identification is nontrivial, as discussed below.

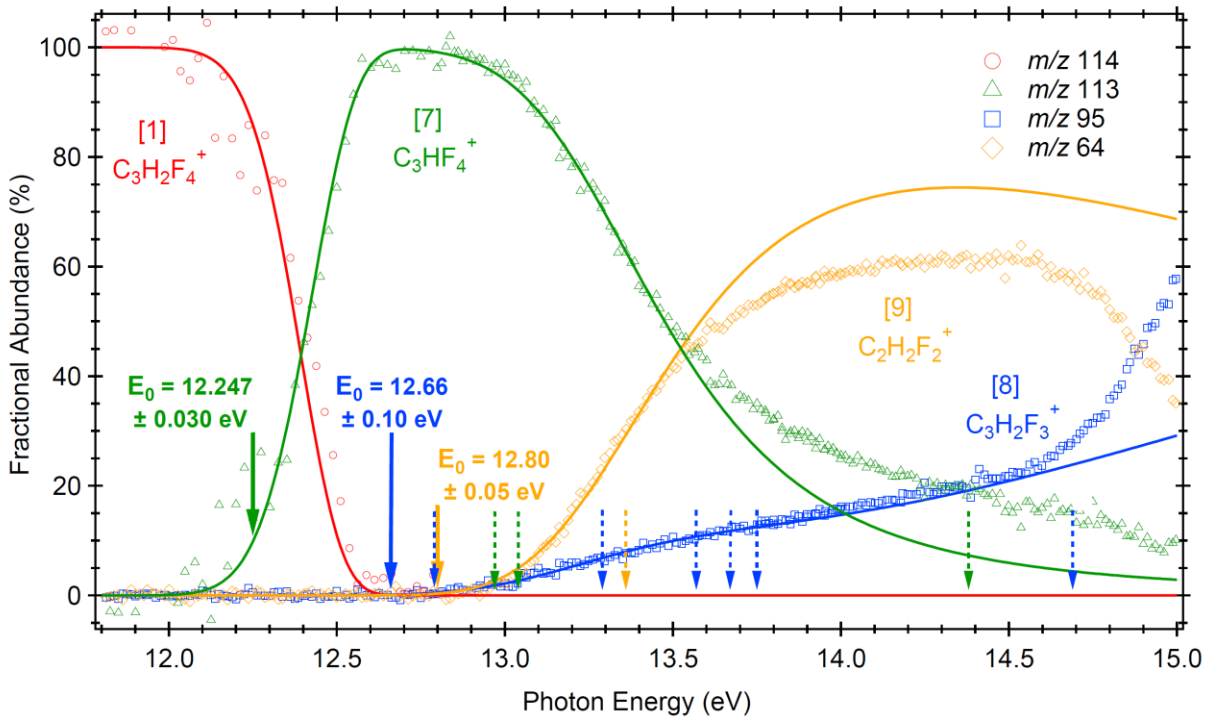

Figure 2. Breakdown diagram of *trans*-1,3,3,3-tetrafluoropropene over the range 11.8–15.0 eV. Experimental data (open shapes) are fit by the modelled breakdown curves (solid lines). Experimental 0 K appearance energies for the three lowest-energy channels are denoted by solid arrows; the various G4-calculated thermochemical limits for the additional pathways are denoted by dashed arrows, as also outlined in Table 2.

Table 1. Summary of experimental and calculated (G4) 0 K appearance energies (E_0) for the lowest-energy 1,3,3,3-tetrafluoropropene fragment pathways.

Fragment Ion	Neutral Fragment	E_0 (eV)	
		Experimental	G4
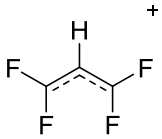 [7]	H	12.247 ± 0.030	12.19
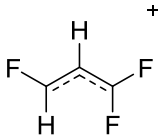 [8]	F	12.66 ± 0.10	12.74
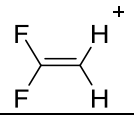 [9]	CF_2	12.80 ± 0.05	13.02

Lowest-Energy Dissociation Channels

The first daughter fragment ion, $C_3HF_4^+$ (*m/z* 113), appears above 12.0 eV in the breakdown diagram. As discussed above, instrumental mass resolution was insufficient for baseline separation of the parent ion $[M]^+$ (*m/z* 114) and the H-loss daughter $[M–1]^+$ (*m/z* 113). Fractional ion abundances and shift in the fragment ion peak center of mass as a function of photon energy were therefore obtained by the Gaussian-fitting deconvolution procedure outlined by Torma *et al.*[30] The resulting breakdown diagram and shifting fragment ion center of mass (which carries metastable dissociation rate information) for the H-loss channel are shown in Figure 3 over the photon range 11.8–12.8 eV. The breakdown curve and fragment ion peak center were modeled using a tight TS and the best fit was obtained by optimization of both barrier height and the two lowest (transitional) vibrational frequencies. The experimental appearance energy for this H-loss channel was found to be 12.247 ± 0.030 eV.

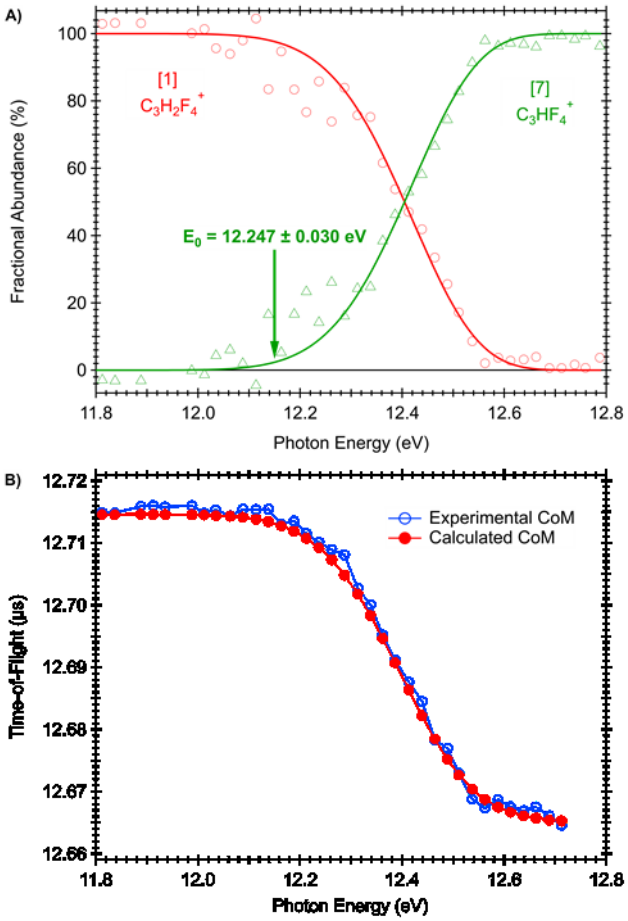

Figure 3. Modeled fit of the H-loss channel in the photon energy range 11.8–12.8 eV, together with the corresponding TOF peak center-of-mass analysis.

Possible dissociative pathways for hydrogen loss are shown in Scheme S1 in the supplementary material; G4 thermochemical limits are summarized in Table 2. Interestingly, although direct hydrogen loss from the parent molecular ion might be expected to be a trivial issue, from the *trans*-1,3,3,3-tetrafluoropropene molecular ion, only one direct H-loss, the one from C1, produces a stable final product. However, with a thermochemical limit of 14.38 eV, this direct-loss channel is substantially too high in energy to explain the experimental data. Therefore, a more stable fragment ion structure must form by rearrangement of the molecular ion. As shown in Figure 4, the lowest-energy pathway involves migration of a fluorine from C3 to C1, passing through barrier $[2]^{‡}$ at 11.95 eV, to form stable intermediate [3] at 11.00 eV. Hydrogen is subsequently lost from C1 through a small barrier $[6]^{‡}$ at 12.17 eV to form a resonantly stabilized allylic cation [7] at 12.05 eV. The calculated thermochemical limit of 12.05 eV with a reverse barrier of 0.12 eV is consistent with the experimental appearance energy of 12.247 ± 0.030 eV. Reversible isomerization of the molecular ion [1] to intermediate [3] was included in the model following the procedure outlined by Li and Baer.[25,39] The isomerization barrier $[2]^{‡}$ and the

transitional vibrational frequencies were optimized, resulting in a loose isomerization barrier prior to the tighter dissociation barrier. However, inclusion of this isomerization step in the statistical model did not produce a superior fit, possibly because the rate determining step is the final one over $[6]^{‡}$. Thus, to avoid over-parameterizing the model, isomerization was omitted from the final statistical model, shown in Figure 3.

Above 12.5 eV, the parallel $C_3H_2F_3^+$ (*m/z* 95) and $C_2H_2F_2^+$ (*m/z* 64) channels open at about the same photon energy. Each channel was modeled using calculated TS frequencies for a loose transition state as a starting point, and the model was fitted to the experimental data by optimizing the transitional vibrational frequencies of each TS and the appearance energy for each channel. The appearance energy for the F-loss channel ($C_3H_2F_3^+$) was determined to be 12.66 ± 0.10 eV and for the CF_2-loss channel ($C_2H_2F_2^+$) to be 12.80 eV ± 0.05 eV. As shown in Figure 2, the model for these channels is in excellent agreement until 13.5 eV, after which it underestimates for *m/z* 113, overestimates for *m/z* 64 and starts to progressively underestimate *m/z* 95. The one channel per fragment ion model does not account for the rapid rise of *m/z* 95 above 14.5 eV, either. As discussed below, various rearrangements open up on the potential energy surface beyond 13 eV, making numerous product formation channels available and thus precluding unambiguous experimental identification of the fragment ions. Therefore, we choose to focus on the lowest-energy channels.

The G4 thermochemical limits for the various possible F-loss $C_3H_2F_3^+$ (*m/z* 95) fragment pathways are summarized in Table 2. As shown in Scheme S2 in the supplementary material, two direct mechanisms are possible for loss of fluorine from the molecular ion: 1) barrierless loss of fluorine from C1 to produce $CHCHCF_3^+$ at 14.69 eV and 2) barrierless loss of fluorine from C3 to produce a more stable allylic cation at 12.74 eV. Alternatively, following the rearrangement pathway observed for the H-loss pathway, fluorine can migrate from C3 to either C1 or C2 prior to dissociation, potentially producing *five* additional allylic cation structures for the $C_3H_2F_3^+$ fragment for a total of six different possible allylic cation structures. The experimental appearance energy of 12.66 ± 0.10 eV is in good agreement with the calculated thermochemical limit of direct F loss leading to allylic cation [8].

For the *m/z* 64 channel, CF_2 cannot be lost directly from the molecular ion; therefore, this channel must include a rearrangement step. The optimized TS in the statistical model is, however, loose, which indicates that this rearrangement probably occurs below the thermochemical limit. The possible fragmentation pathways are shown in Figure S3. Each involves a transfer of fluorine from C3 to one of the other carbons to form a stable intermediate, from which neutral CF_2 can be lost by barrierless C–C bond scission. The thermochemical limits for the formation of *cis*-, *trans*-, and 1,1-difluoroethene cations are included in Table 2. Of these, the 1,1-difluoroethene cation is the most stable, with a G4 thermochemical limit of 13.02 eV, in reasonable agreement with the experimental appearance energy of 12.80 eV ± 0.05 eV. Formation of the 1,1-difluoroethene cation proceeds through the same stable intermediate [3] as for the H-loss channel but undergoes additional H-atom migration prior to dissociation, as shown in Figure 4.

The discrepancy of 0.22 eV between experimental and calculated appearance energies still falls within the limit of the overlap in error bars between the two. We therefore remain confident in our assignment of 1,1-difluoroethene to the *m/z* 64 channel. Additionally, there are only a limited number of possible $C_2H_2F_2$ fragment ions, and all other products would appear at higher energies, as shown in Table 2.

3. Computational Results and Higher-Energy Pathways

Analysis of the experimental data was complemented and aided by *ab initio* quantum chemical calculations on the cationic potential energy surface. Preliminary calculations used to identify the most likely pathways were carried out at B3LYP/6-311++G(d,p) level of theory. Transition states and reaction mechanisms were identified by scanning along the internal coordinates. The energies of the stationary points of interest were further refined by the G4 composite method.[35] All direct and indirect dissociation pathways are shown in schemes S1–S3 in the supplementary materials and a summary of their thermochemical limits is provided in Table 2. Finally, the 0 K G4 energies relative to the neutral for the lowest-energy pathways corresponding to those used in the model are shown in Figure 4.

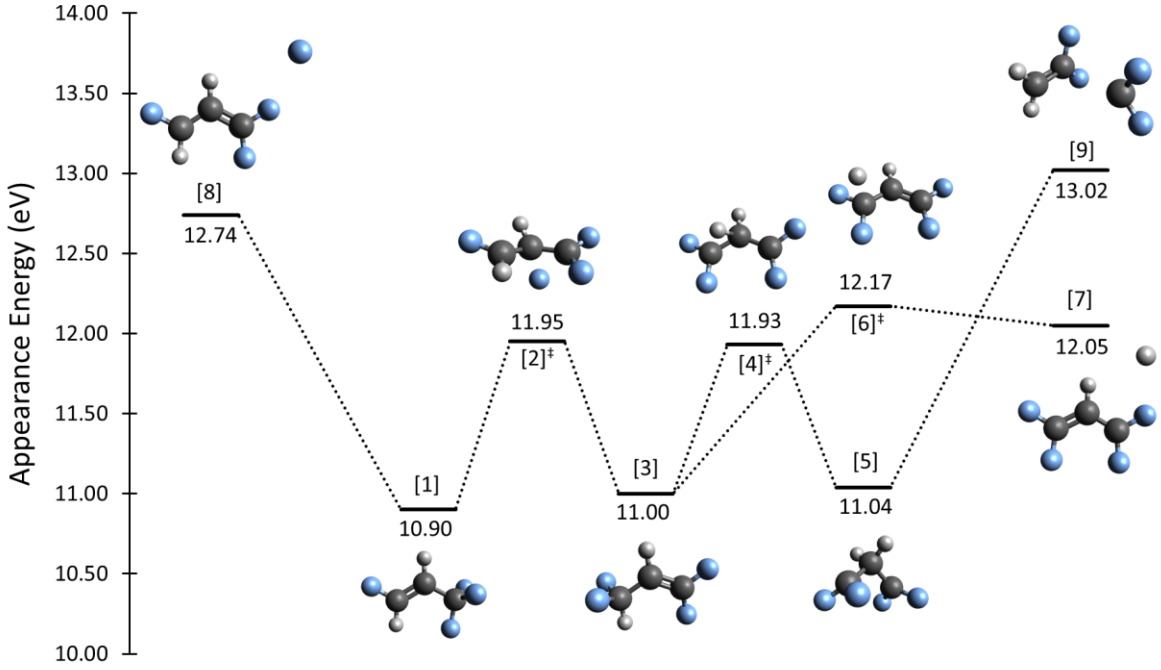

Figure 4. Potential energy surface for the lowest-energy dissociation pathways from the *trans*-1,3,3,3-tetraflluoropopene cation [1]. All energies are at 0 K, calculated at the G4 level of theory, and are presented relative to the neutral precursor.

Table 2. Calculated thermochemical limits relative to the neutral precursor calculated at the G4 level of theory.

Fragments		Thermochemical Limit (eV)	Fragments		Thermochemical Limit (eV)
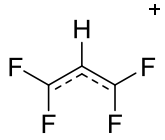	[7] + H	12.05	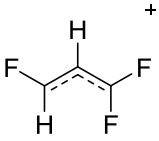	[8] + F	12.74
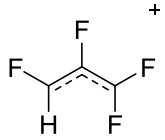	[10] + H	12.97	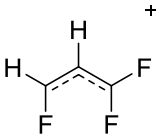	[13] + F	12.79
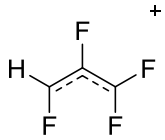	[11] + H	13.04	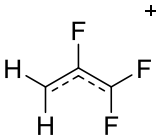	[14] + F	13.29
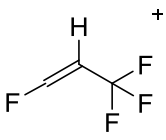	[12] + H	14.38	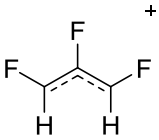	[15] + F	13.57
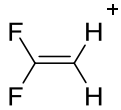	[9] + CF_2	13.02	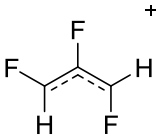	[16] + F	13.67
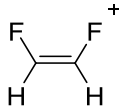	[19] + CF_2	13.36	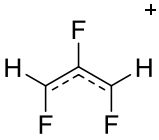	[17] + F	13.75
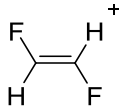	[20] + CF_2	13.36	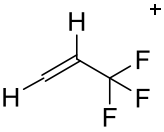	[18] + F	14.69

As shown in Figure 4, all three lowest-energy pathways involve removal of a fluorine from C3. The F-loss channel can arise in two ways: 1) a fluorine can be lost directly by C–F bond scission to form allylic cation [8] or, alternatively, 2) a fluorine can be transferred from C3 to C1 via a four-member ring TS $[2]^{‡}$ to form stable intermediate [3]. In the latter case, the intermediate can then either 1) lose a hydrogen by passing through a reverse barrier $[6]^{‡}$ to form allylic cation [7] or 2) transfer the hydrogen from C1 to C3 via the three-member ring TS $[4]^{‡}$ to form another stable intermediate [5], then undergo barrierless C–C scission to form a 1,1-difluoroethene cation and neutral CF_2. Note that, because intermediate [5] is not planar, it can form both *cis*- and *trans*-difluoroethene cations, despite starting with the *trans*- form of the molecular ion. However, both additional difluoroethene cations are calculated to have greater appearance energies than does the 1,1-difluoroethene cation, as summarized in Table 2.

Additional Dissociation Channels

As discussed above, the experimental breakdown diagram (Figure 2) is well modeled up to 13.5 eV by three parallel dissociative pathways, one for each fragment ion. Above this point, the model underestimates the *m/z* 113 and overestimates the *m/z* 64 channel. This strongly indicates that additional dissociation pathways open up in this energy range. Furthermore, beyond 14.5 eV, an unexplained and very rapid rise in the F-loss fragment ion signal was observed, indicating that new fluorine atoms loss channel(s) suddenly become highly competitive. The 0 K thermochemical limits calculated at the G4 level of theory for additional fragmentation pathways are summarized in Table 2 and denoted by dashed arrows on the breakdown diagram in Figure 2.

Possible H-loss pathways are shown in Scheme S1 in the supplementary materials; the thermochemical limits are summarized in Table 2. From these, there are two available pathways leading to allylic cations [10] and [11] with calculated appearance energies around 13 eV. Both daughter fragments may be formed by first transferring a fluorine from C3 to C2 through a three-member ring barrier to form a stable intermediate. This initial fluorine transfer barrier is 0.24 eV higher in energy than that for transfer of fluorine from C3 to C1 observed in the lowest-energy pathway, as might be expected for a three-member ring structure vs. a four-member ring structure. Prior to the loss of hydrogen, there is an additional hydrogen-migration step whereby the hydrogen on C2 hops over to either C1 or C3 through higher but still submerged barriers. Finally, hydrogen is lost by barrierless C–H bond scission to form the additional allylic cation structures. Given how close allylic cations [10] and [11] are in energy, it is impossible to distinguish unambiguously between them experimentally. But the increased abundance of the *m/z* 113 channel at higher photon energies can be attributed to at least one of these pathways.

The model for the F-loss channel is consistent with the lowest-energy fluorine loss and describes the fractional ion abundance signal for the *m/z* 95 channel well below 14.5 eV. Above this energy, additional F-loss channels are needed to fit the breakdown diagram, but their identification is nontrivial. In addition to the direct-loss mechanism observed for the lowest-energy channel, fluorine loss may compete with hydrogen-loss and CF_2-loss from the intermediates formed by fluorine migration from C3 to either C1 or C2 to form additional allylic cation fragments. These additional F-loss pathways are shown in Scheme S2 in the supplementary material; the thermochemical limits are summarized in Table 2. With a total of six different allylic cation fragments available within 1 eV of each other, it is impossible to state with any certainty which additional pathways are present. Additionally, as shown in Scheme S2, the lowest-energy F-loss allylic cation [8] produced by direct C–F bond scission can also be formed by both fluorine-migration pathways. These pathways proceed through small barriers, which means that, at higher ion internal energies, the potential energy surface of the various isomers becomes strongly coupled, fluorine loses its locational identity, and is largely free to roam between the various carbon sites. Therefore, although these additional dissociation pathways are clearly present, it is not possible to unambiguously identify which pathways are contributing how much

to the rapid rise in the experimental F-loss signal. In fact, the strong increase in signal above 14.5 eV is likely the result of not a single additional F-loss pathway, but the presence of many F-loss pathways generally outcompeting the other fragmentation pathways.

Thermochemistry

For dissociative photoionization, the 0 K appearance energy of the fragment ion is equivalent to the thermochemical limit in the absence of a reverse barrier. Thus, the E_0 for such fragmentations can be used to connect the heats of formation of the fragmentation products to those of the neutral precursor. On one hand, the H-loss channel proceeds through a small reverse barrier and is therefore unsuitable for thermochemistry. On the other hand, according to theory, the 0 K appearance energies for both the lowest-energy F-loss and CF_2-loss channels correspond to their respective thermochemical limits, despite the substantial rearrangement required to form the CF_2 leaving group, and can therefore be used to extract reliable thermochemical information on the heat of formation of the parent neutral, parent molecular ion, and daughter fragments by means of the thermochemical cycles shown in Figure 5. Ancillary thermochemical data and the results of this work are summarized in Table 3.

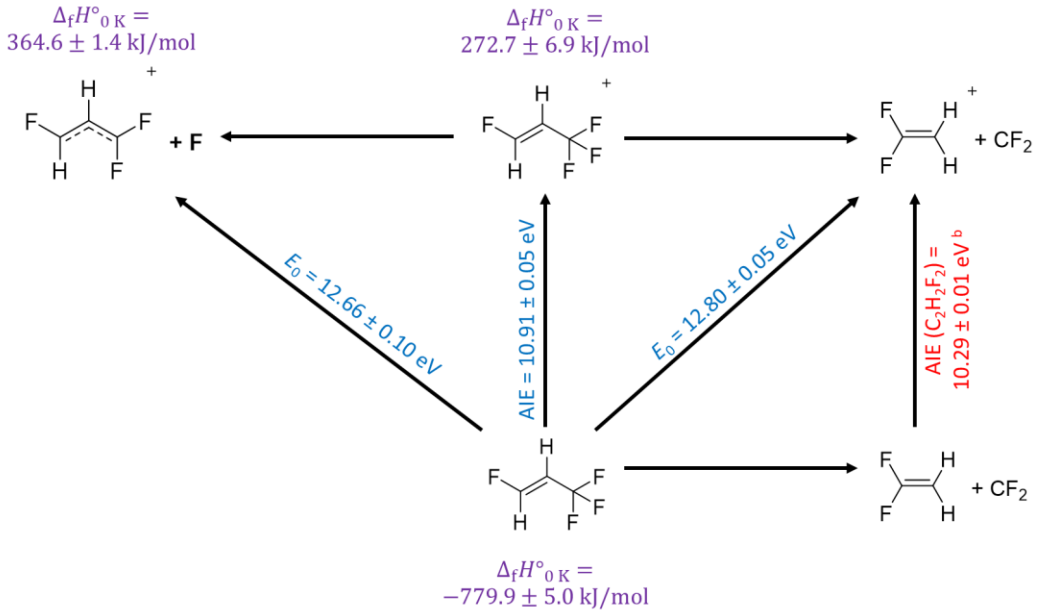

Figure 5. Positive ion thermochemical cycles of the *trans*-1,3,3,3-tetrafluoropropene system for the F-loss pathway (left) and the CF_2-loss pathway (right). The ionization energy of *trans*-1,3,3,3-tetrafluoropropene and the appearance energies for both pathways, shown in blue, are measured experimentally in this work. New thermochemical values determined in this work are shown in purple; 0 K heats of formation[38] used in these cycles are included in Table 3.

Table 3. Auxiliary and derived thermochemical data

Chemical Formula	Species	$\Delta_f H^\circ_{0\ K}$ (kJ mol^{-1})	$\Delta_f H^\circ_{298\ K}$ (kJ mol^{-1})	Uncertainty (kJ mol^{-1})
$C_3H_2F_4$	*trans*-1,3,3,3-tetrafluropropene	-779.9[a] -803.1 to -831.8[c,f]	-783.8 to -812.5[c]	± 5.0 ± 8.5
$C_3H_2F_4^+$	*trans*-1,3,3,3-tetrafluropropene cation	272.7[a]		± 6.9
$C_3H_2F_3^+$	allylic cation [8]	364.6[a]		± 1.4
$C_2H_2F_2$	1,1-difluoroethene	-343.65[b]	-350.72[b]	± 0.82
$C_2H_2F_2^+$	1,1-difluoroethene cation	649.3[e]		± 1.3
CF_2	diflourocarbene	-193.93[b] -205.4[d,f]	-193.46[b] -195.0[d]	± 0.38 ± 2.9
F	fluorine atom ($^2P_{3/2}$)	77.255[b]	79.361[b]	± 0.048

[a]This work; [b]Active Thermochemical Tables (ATcT)[38]; [c]Demenay *et al.* calculated values at PM3 to B3LYP levels of theory[40]; [d]Feller and Dixon[41]; [e]Value calculated from $\Delta_f H^\circ_{0\ K}(C_2H_2F_2)$[38] and AIE = 10.29 ± 0.01 eV[42]; [f]Converted to *T* = 0 K using G4 thermal values.

Although CF_2-loss involves substantial rearrangement prior to dissociation, the barriers to rearrangement are submerged, and therefore the experimental appearance energy corresponds to the thermochemical limit. Starting with the heat of formation of neutral 1,1-difluoroethene and using the known IE for this species of 10.29 ± 0.01 eV[42], a value of $\Delta_f H^\circ_{0\ K}(C_2H_2F_2^+)$ = 649.3 ± 1.3 kJ/mol is obtained for the 1,1-difluoroethene cation. Using this value in conjunction with $\Delta_f H^\circ_{0\ K}(CF_2) = -193.93 \pm 0.38$ kJ/mol[38] and the experimentally obtained E_0 = 12.80 ± 0.05 eV we determine a value of $\Delta_f H^\circ_{0\ K}(C_3H_2F_4) = -779.9 \pm 5.0$ kJ/mol for the neutral precursor *trans*-1,3,3,3-tetrafluoropropene. Previous semi-empirical (PM3, PM6, PM7) and *ab initio* (B3LYP) calculations from Demenay *et al.* predict $\Delta_f H^\circ_{0\ K}(C_3H_2F_4)$ values from -803.1 to -838.8 kJ/mol,[40] which are mostly consistent with our experimental value, taking their expected accuracy into account but highlighting some of the issues with obtaining accurate energetics on fluorinated species from theory alone. Expanding on our experimental value of $\Delta_f H^\circ_{0\ K}(C_3H_2F_4)$ and using our experimental value for *trans*-1,3,3,3-tetrafluoropropene of AIE = 10.91 ± 0.05 eV, we can also determine, for the molecular ion, a value of $\Delta_f H^\circ_{0\ K}$ = 272.7 ± 6.9 kJ/mol. To our knowledge, the heat of formation for the *trans*-1,3,3,3-tetrafluoropropene cation has not previously been reported in literature.

Finally, using the experimental appearance energy difference between the CF_2-loss (12.66 eV) and F-loss (12.80 eV) channels, ΔE_0 = 0.14 ± 0.04 eV, the known $\Delta_f H^\circ_{0\ K}(CF_2) = 193.93 \pm 0.38$ kJ/mol,[38] and the known $\Delta_f H^\circ_{0\ K}(F) = 77.255 \pm 0.048$ kJ/mol,[38] we obtain a 0 K heat of

formation for the allylic $C_3H_2F_3^+$ fragment [8] as 364.6 ± 1.4 kJ/mol. Simpson and Tuckett previously published possible upper limits of $\Delta_f H^\circ_{0\,K}$ <395 kJ/mol and <421 kJ/mol for the formation of CHF=CH-CF_2^+ (presumed structure) formed by reaction of $C_2F_4^+ +$ C_2H_3F or CH_2F_2.[43] Our new value, based not on an absolute appearance energy but rather on a more accurate relative value, offers a substantial improvement over these early estimates.

Conclusion

We present herein the first experimental threshold photoelectron spectrum and dissociative photoionization data for *trans*-1,3,3,3-tetrafluoropropene. Based on the TPES and a Franck–Condon simulation, we determine an experimental AIE of 10.91 ± 0.05 eV. In dissociative photoionization, we observed three fragment masses: *m/z* 113, *m/z* 95, and *m/z* 64, corresponding to loss of H, F, and CF_2, respectively. Interestingly, although photoionization can involve direct H-loss, a more energetically favorable route starts by rearrangement by fluorine and hydrogen migration, followed by dissociation to form an allylic cation [9]. This happens to be a recurring theme for the other dissociation pathways as well: the vagabond nature of the fluorine atom, due to the strongly coupled nature of the potential energy surface of various isomeric species at higher energies, opens several possible pathways to dissociation. While the lowest-energy F-loss channel involves direct-loss of fluorine from C3, several additional F-loss channels fall within 1.5 eV of this first channel, and all involve both fluorine and hydrogen migration to form various stable allylic cation fragments. Finally, the CF_2 fragment must be formed by similar rearrangements of the molecular ion, with the lowest-energy pathway forming the 1,1-difluoroethene cation. This is a useful thermochemical anchor, which enabled us to determine the experimental heat of formation for *trans*-1,3,3,3-tetrafluoropropene as $\Delta_f H^\circ_{0\,K}(C_3H_2F_4) = -779.9 \pm 5.0\ \mathrm{kJ/mol}$.

Acknowledgements

This work was funded by the National Science Foundation (grant no. CHE-1665464).

Supporting Information

Schemes for hydrogen-loss, fluorine-loss and CF_2-loss pathways.

References

1. Molina, M. J.; Rowland, F. S. Stratospheric sink for chlorofluoromethanes: chlorine atom-catalysed destruction of ozone. *Nature* **1974***, 249*, 810-812.

2. Guus J. M. Velders; Stephen O. Andersen; John S. Daniel; David W. Fahey; Mack McFarland The Importance of the Montreal Protocol in Protecting Climate. *Proceedings of the National Academy of Sciences of the United States of America* **2007***, 104*, 4814-4819.

3. Abas, N.; Kalair, A. R.; Khan, N.; Haider, A.; Saleem, Z.; Saleem, M. S. Natural and synthetic refrigerants, global warming: A review. *Renewable and Sustainable Energy Reviews* **2018***, 90*, 557-569.

4. Antiñolo, M.; Bravo, I.; Jiménez, E.; Ballesteros, B.; Albaladejo, J. Atmospheric Chemistry of E- and Z-$CF_3CH{=}CHF$ (HFO-1234ze): OH Reaction Kinetics as a Function of Temperature and UV and IR Absorption Cross Sections. *J Phys Chem A* **2017***, 121*, 8322-8331.

5. Wallington, T. J.; Sulbaek Andersen, M. P.; Nielsen, O. J. Atmospheric chemistry of short-chain haloolefins: Photochemical ozone creation potentials (POCPs), global warming potentials (GWPs), and ozone depletion potentials (ODPs). *Chemosphere* **2015***, 129*, 135-141.

6. Wuebbles, D. J.; Wang, D.; Patten, K. O.; Olsen, S. C. Analyses of new short-lived replacements for HFCs with large GWPs. *Geophys. Res. Lett.* **2013***, 40*, 4767-4771.

7. Matsugi, A.; Takahashi, K. Thermal Decomposition of 2,3,3,3- and trans-1,3,3,3-Tetrafluoropropenes. *J Phys Chem A* **2017***, 121*, 4881-4890.

8. Søndergaard, R.; Nielsen, O. J.; Hurley, M. D.; Wallington, T. J.; Singh, R. Atmospheric chemistry of trans-CF_3CHCHF: Kinetics of the gas-phase reactions with Cl atoms, OH radicals, and O_3. *Chemical Physics Letters* **2007***, 443*, 199-204.

9. Orkin, V. L.; Martynova, L. E.; Ilichev, A. N. High-Accuracy Measurements of OH Reaction Rate Constants and IR Absorption Spectra: $CH_2{=}CF{-}CF_3$ and trans-$CHF{=}CH{-}CF_3$. *The Journal of Physical Chemistry A* **2010***, 114*, 5967-5979.

10. Balaganesh, M.; Rajakumar, B. Rate Coefficients and Reaction Mechanism for the Reaction of OH Radicals with (E)-$CF_3CH{=}CHF$, (Z)-$CF_3CH{=}CHF$, (E)-$CF_3CF{=}CHF$, and (Z)-$CF_3CF{=}CHF$ between 200 and 400 K: Hybrid Density Functional Theory and Canonical Variational Transition State Theory Calculations. *J Phys Chem A* **2012***, 116*, 9832-9842.

11. Zhang, N.; Chen, L.; Mizukado, J.; Quan, H.; Suda, H. Rate constants for the gas-phase reactions of (Z)-CF_3CHCHF and (E)-CF_3CHCHF with OH radicals at 253–328K. *Chemical Physics Letters* **2015***, 621*, 78-84.

12. Peers, M.; Vigny, P. N° 64. — Réactions molécule-ion dans le propylène. *J.Chim.Phys.* **1968***, 65*, 805-815.

13. Haney, M. A.; Franklin, J. L. Correlation of Excess Energies of Electron-Impact Dissociations with the Translational Energies of the Products. *The Journal of Chemical Physics* **1968***, 48*, 4093-4097.

14. Kräßig, R.; Reinke, D.; Baumgärtel, H. Photoreaktionen kleiner organischer Moleküle II. Die Photoionenspektren der Isomeren Propylen-Cyclopropan und Acetaldehyd-Äthylenoxyd. *Berichte der Bunsengesellschaft für physikalische Chemie* **1974***, 78*, 425-436.

15. Buttrill, S. E.; Williamson, A. D.; LeBreton, P. Photoionization measurement of the heat of formation of allyl cations. *J. Chem. Phys.* **1975***, 62*, 1586-1587.

16. Traeger, J. C. A study of the allyl cation thermochemistry by photoionization mass spectrometry. *International Journal of Mass Spectrometry and Ion Processes* **1984***, 58*, 259-271.

17. Berman, D. W.; Bomse, D. S.; Beauchamp, J. L. Photoionization threshold measurements for CF_2 loss from perfluoropropylene, perfluorocyclopropane, and trifluoromethylbenzene. The heat of formation of CF_2 and consideration of the potential-energy surface for interconversion of isomeric C_3F_6 neutrals and ions. *International Journal of Mass Spectrometry and Ion Physics* **1981***, 39*, 263-271.

18. Lifshitz, C.; Long, F. A. Appearance Potentials and Mass Spectra of C_3F_6, C_3F_5Cl, and c-C_3F_6. *J. Phys. Chem.* **1965***, 69*, 3741-3746.

19. Jarvis, G. K.; Boyle, K. J.; Mayhew, C. A.; Tuckett, R. P. Threshold Photoelectron−Photoion Coincidence Spectroscopy of Perfluorocarbons. 2. Unsaturated and Cyclic Perfluorocarbons C_2F_4, C_3F_6, 2-C_4F_8, and c-C_4F_8. *J Phys Chem A* **1998***, 102*, 3230-3237.

20. Harvey, J.; Bodi, A.; Tuckett, R. P.; Sztáray, B. Dissociation dynamics of fluorinated ethene cations: from time bombs on a molecular level to double-regime dissociators. *Phys. Chem. Chem. Phys.* **2012***, 14*, 3935-3948.

21. Johnson, M.; Bodi, A.; Schulz, L.; Gerber, T. Vacuum ultraviolet beamline at the Swiss Light Source for chemical dynamics studies. *Nuclear Instruments and Methods in Physics Research Section A: Accelerators, Spectrometers, Detectors and Associated Equipment* **2009***, 610*, 597-603.

22. Bodi, A.; Johnson, M.; Gerber, T.; Gengeliczki, Z.; Sztáray, B.; Baer, T. Imaging photoelectron photoion coincidence spectroscopy with velocity focusing electron optics. *Rev. Sci. Instrum.* **2009***, 80*, 034101.

23. Bodi, A.; Sztáray, B.; Baer, T.; Johnson, M.; Gerber, T. Data acquisition schemes for continuous two-particle time-of-flight coincidence experiments. *Rev. Sci. Instrum.* **2007***, 78*, 084102.

24. Sztáray, B.; Baer, T. Suppression of hot electrons in threshold photoelectron photoion coincidence spectroscopy using velocity focusing optics. *Rev. Sci. Instrum.* **2003***, 74*, 3763-3768.

25. Sztáray, B.; Bodi, A.; Baer, T. Modeling unimolecular reactions in photoelectron photoion coincidence experiments. *Journal of mass spectrometry* **2010***, 45*, 1233-1245.

26. Baer, T.; Sztáray, B.; Kercher, J. P.; Lago, A. F.; Bödi, A.; Skull, C.; Palathinkal, D. Threshold photoelectron photoion coincidence studies of parallel and sequential dissociation reactions. *Physical chemistry chemical physics : PCCP* **2005***, 7*, 1507-1513.

27. Benson, S. W. Thermochemical Kinetics: Methods for the Estimation of Thermochemical Data and Rate Parameters. **1976**.

28. Voronova, K.; Mozaffari Easter, C. M.; Covert, K. J.; Bodi, A.; Hemberger, P.; Sztáray, B. Dissociative Photoionization of Diethyl Ether. *The Journal of Physical Chemistry A* **2015***, 119*, 10654-10663.

29. Bodi, A.; Daniel Brannock, M.; Sztáray, B.; Baer, T. Tunneling in H loss from energy selected ethanol ions. *Physical chemistry chemical physics : PCCP* **2012***, 14*, 16047-16054.

30. Torma, K. G.; Voronova, K.; Sztáray, B.; Bodi, A. Dissociative Photoionization of the C_7H_8 Isomers Cycloheptatriene and Toluene: Looking at Two Sides of the Same Coin Simultaneously. *The Journal of Physical Chemistry A* **2019***, 123*, 3454-3463.

31. Frisch, M. J.; Trucks, G. W.; Schlegel, H. B.; Scuseria, G. E.; Robb, M. A.; Cheeseman, J. R.; Scalmani, G.; Barone, V.; Mennucci, B.; Petersson, G. A., et al. Gaussian 09. **2009**.

32. Peng, C.; Bernhard Schlegel, H. Combining Synchronous Transit and Quasi-Newton Methods to Find Transition States. *Israel Journal of Chemistry* **1993***, 33*, 449-454.

33. Peng, C.; Ayala, P. Y.; Schlegel, H. B.; Frisch, M. J. Using redundant internal coordinates to optimize equilibrium geometries and transition states. *Journal of Computational Chemistry* **1996***, 17*, 49-56.

34. Fukui, K. The path of chemical reactions - the IRC approach. *Accounts of Chemical Research* **1981***, 14*, 363-368.

35. Curtiss, L.; Redfern, P.; Raghavachari, K. Gaussian-4 theory. *Journal of Chemical Physics* **2007***, 126*, 084108-12.

36. Baer, T.; Hase, W. L. *Unimolecular reaction dynamics: theory and experiments;* Oxford University Press: New York, 1996; , pp 438.

37. Beyer, T.; Swinehart, D. Algorithm 448: number of multiply-restricted partitions. *Communications of the ACM* **1973***, 16*, 379.

38. Rustic, B.; Bross, D. H. Active Thermochemical Tables (ATcT) Version 1.122e. *ATcT.anl.gov* (accessed February 28, 2019).

39. Li, Y.; Baer, T. Ethylene Glycol Ions Dissociate by Tunneling through an H-Atom Transfer Barrier: A DFT and TPEPICO Study. *J Phys Chem A* **2002***, 106*, 8658-8666.

40. Demenay, A.; Glorian, J.; Paricaud, P.; Catoire, L. Predictions of the ideal gas properties of refrigerant molecules. *International Journal of Refrigeration* **2017***, 79*, 207-216.

41. Dixon, D. A.; Feller, D. Heats of Formation of CF_2, FCO, and CF_2O. *The Journal of Physical Chemistry A* **1998***, 102*, 8209-8216.

42. Bieri, G.; von Niessen, W.; Åsbrink, L.; Svensson, A. The He(II) photoelectron spectra of the fluorosubstituted ethylenes and their analysis by the Green's function method. *Chemical Physics* **1981***, 60*, 61-79.

43. Simpson, M. J.; Tuckett, R. P. Selected Ion Flow Tube Study of the Gas-Phase Reactions of CF^+, CF_2^+, CF_3^+, and $C_2F_4^+$ with C_2H_4, C_2H_3F, CH_2CF_2, and C_2HF_3. *The Journal of Physical Chemistry A* **2012***, 116*, 8119-8129.